Supplemental Information

1 Methods – Site-Specific Simulation

Microstructural properties ascribed to the site-specific simulation firn column are provided in Table S1.

Table S1: Initial microstructure parameters of the site-specific simulation firn column. Values are uniform across the entire profile initially.

Parameter	Value
Grain radius, all layers (mm)	0.8†
Bond radius, all layers (mm)	0.25
Dendricity, all layers	0
Sphericity, all layers	0.5
Microstructure parameter ('mk', categorical)	1 (indicates that snow has become faceted)

† A grain radius of 0.8mm produces firn grains with sizes slightly smaller than those reported by McDowell et al. (2023)

2 Methods – Synthetic Simulations

2.1 Spin up

The model was initialized with a 15m-deep synthetic firn profile using the Herron and Langway formulation for increasing firn density with depth (Herron and Langway, 1980), assuming a constant new snow density of 315 kg m^{-3} (Fausto et al., 2018; Howat, 2022) mean annual accumulation rate of 0.4m w.e. yr^{-1} (RACMO, Noël, 2019), and pure ice density of 917 kg m^{-3}. A vertical temperature profile and lower Dirichlet boundary condition of -16.5°C (Saito et al., 2024) was ascribed to the firn column, the MAAT of site CP-1998m. Universal microstructural parameters reflective of percolation zone properties were also provided (Table S2). The spin up was forced with a sinusoidal air temperature curve with a 1-year wavelength starting/ending on April 1st, amplitude of 14.5°C, max temperature of -2°C and minimum of -31°C. All other inputs were set constant except precipitation, which occurred randomly and amounted to 0.4-0.5m w.e. yr^{-1} (Table S2). Forcings were provided at hourly timesteps.

2.2 Synthetic Wetting Front Simulation

The spin-up output on April 1st was used as the starting firn profile for the transient run. Average hourly air temperature (GC-NET PROMICE, Steffen et al., 2022) over the calendar year was computed and fit with a sinusoidal, year-length temperature curve and a secondary, diurnally fluctuating sinusoid (Fig. S1). Longwave radiation (LWR) was calculated directly from temperature using the Stefan-Boltzmann Law. Shortwave radiation (SWR) values were also averaged hourly and trimmed with two sinusoidal envelopes to smooth local minima and maxima (Fig. S1). Winter SWR values were set to 0 (Fig. S1).

Precipitation occurred randomly and amounted to 0.5m w.e. yr^{-1}. Wind speed, direction, and relative humidity were set equal to spin-up values (Fig. S1). SNOWPACK was configured identically to the site-specific simulation.

Table S2: Firn profile initial conditions and meteorological forcings, spin-up period for synthetic simulations.

Initial Conditions – Microstructure	**Value**
Grain radius (mm)	0.75
Bond radius (mm)	0.5
Dendricity	0 ('old' snow)
Sphericity	0.6
Microstructure marker ('mk')	1 (meaning grains have become faceted')
Stress change rate	0
Site Information	**Value**
Site altitude	1998m
Site coordinates	69.872469, -47.036429
Meteorological Forcings	**Value**
Shortwave radiation (W m^{-2})	2
Longwave radiation (W m^{-2}) †	300
Precipitation (m yr^{-1})	0.4-0.5, occuring randomly
Windspeed (m s^{-1})	3
Wind direction	20
Relative humidity	0.61

† A LWR value of 300 W m^{-2} was determined using the Stefan-Boltzmann Law ($I = \varepsilon\sigma T^4$), which assumes no cloud influence. This value balances heat fluxes during the spinup to retain a vertical deep-firn temperature profile at -16.5℃.

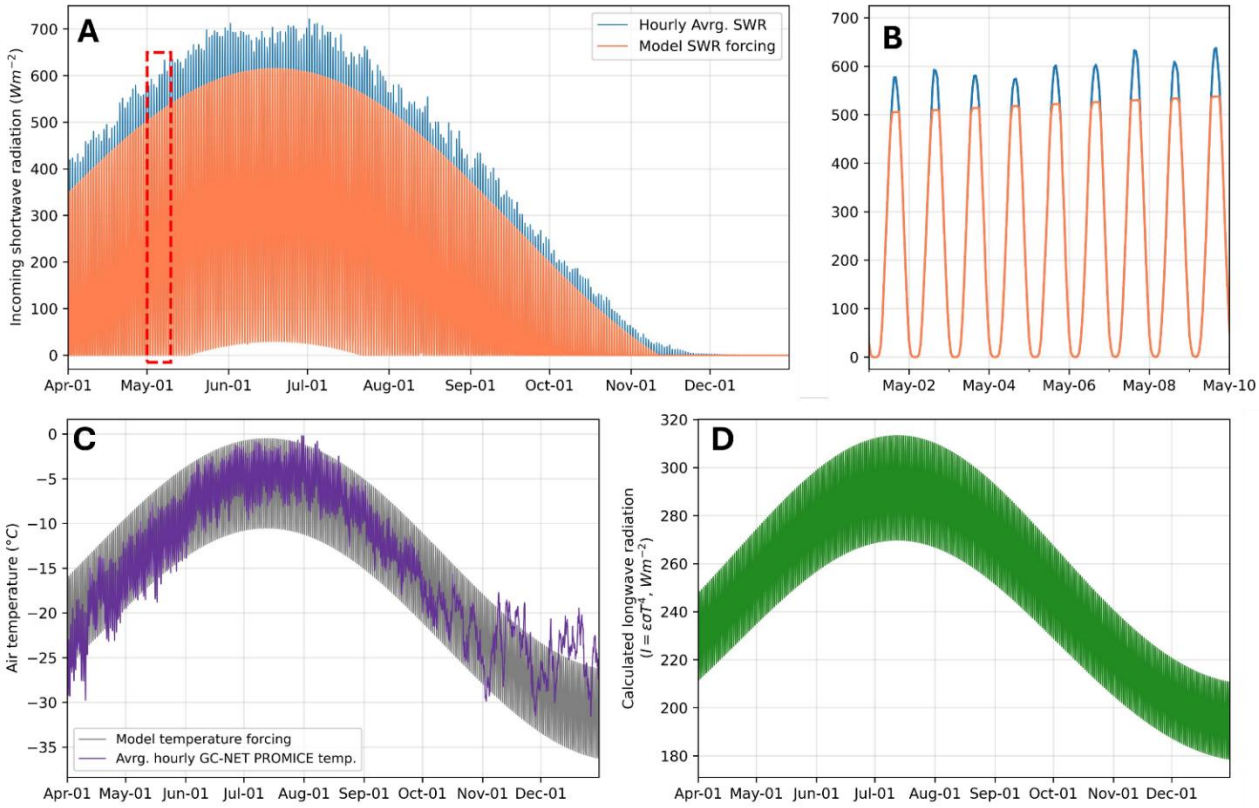

Figure S1: Meteorological forcings employed in the synthetic Wetting Front and Preferential Flow (Piping) simulations. Forcings span from April 1st – December 31st. A) Measured hourly average shortwave radiation values from 1995-2020 at the GC-NET PROMICE weather station, site CP-1998m (blue line). Model SWR forcings were created by trimming local maxima and minima with two envelopes (orange line). The data within the red dashed box are shown in B), a close-up of diurnal fluctuations in the shortwave radiation data/model forcing. C) Measured hourly average air temperature data from 1995-2020 (purple line), also from the CP-1998m weather station. Averages were fit with a sinusoid with a secondary, diurnally fluctuating sinusoid (grey line) to capture approximate air temperature fluctuations throughout the year. Using the sinusoidal air temperature forcings, we directly calculated longwave radiation (D) from temperature using the Stefan-Boltzmann Law.

2.3 Synthetic Preferential Flow (Piping) simulation

The spin-up output on July 1st was used as the starting firn profile for the liquid water layer perturbation. Three microstructural parameters – grain radius, sphericity, and 'mk' – within the spin-up output were edited prior to perturbation. Grain sizes were universally increased by a factor of 1.5x across the firn column to better reflect percolation zone properties. Sphericity values were set to 0.5. The 'mk' microstructural parameter (SNOWPACK marker, see Lehning et al. (2002b)) was set to 1, indicating snow had become faceted. All other firn parameters were retained from the July 1st spin-up output. We acknowledge the average % liquid water in piping events is unknown, but the heat signature and final layer density (~890 kg m^{-3}) generated from the properties of the inserted liquid water layer reflect observations.

3 Results

Site-by-site characteristics, as well as overall site averages, of the two meltwater-induced faceting modes, wet layer onset and preferential flow/piping, are found in Table S3.

Table S1: Duration, timing, and depths of observed wet layer onset and preferential flow/piping Critical Temperature Gradients (CTGs, ≥|±10| ℃ $\mathbf{m^{-1}}$) at various sites. Only those sites experiencing either form of CTG are included.

Site I.D.	Msrmt. year	Wet layer CTG date range †		Wet lyr. CTG duration (hrs)‡	Wet lyr. CTG depth ranges (m)		# of piping CTG events•	Piping CTG duration (hrs)‡	Piping CTG depth ranges (m)	
Site Averages	-	-	-	**263.94**	**0.67**	**3.31**	-	**45.47**	**2.42**	**6.06**
H3-1540m	2008	6/13/2008	7/16/2008	198	1	3.25	1	19.00	2.00	4.75
H2-1555m	2008	6/9/2008	7/20/2008	253	0.25	5.00	1	22.00	4.00	5.25
H1-1680m	2008	6/14/2008	7/17/2008	83	0.50	2.25	1	22.50	2.50	5.25
H163-1660m	2008	6/14/2008	7/12/2008	76	0.75	3.00	1	12.00	2.25	4.25
H165-1680m	2008	6/14/2008	8/19/2008	56.5	0.50	3.00	1	12.50	2.25	5.25
T1-1710m	2008	6/14/2008	8/4/2008	100.5	0.25	3.75	1	18.50	2.00	3.75
T2-1750m	2007	6/28/2007	8/4/2007	191.5	0.75	5.00	1	96.50	3.50	17.0
T3-1818m	2007	6/25/2007	8/9/2007	86.5	1.50	3.50	2	120.50	4.00	5.25
T3-1818m, 15m core	2022	7/5/2022	9/9/2022	960	0.13	3.50	1	110.00	1.50	4.50
T3-1818m, 25m core	2022	7/6/2022	9/11/2022	407.5	0.25	4.50	2	42.00	1.75	9.00
T4-1878m	2007	7/3/2007	8/1/2007	268.5	0.75	3.00	1	4.50	1.00	9.00
T4-1878m	2022	7/6/2022	8/5/2022	260	0.25	1.25	1	3.00	0.75	3.00
T4-1878m	2023	7/9/2023	7/23/2023	155	1.50	3.75	1	2.00	5.00	6.00
T5-1928m	2023	7/10/2023	7/22/2023	157.5	0.75	4.00	1	190.00	2.25	7.75
CP-1998m	2007	6/25/2007	7/28/2007	603	0.75	2.25	-	-	-	-
CP-1998m	2023	7/6/2023	7/18/2023	226.5	1.25	2.75	1	44.00	2.50	4.75
UP18-2102m	2023	7/8/2023	7/29/2023	504	0.25	2.50	1	8.50	1.50	2.25

† Date ranges encompass the minimum and maximum dates in which CTGs associated with wet layer onset were observed. CTGs were not necessarily observed continuously over the specified range.

‡ Temperature gradient durations are the cumulative time in which temperature gradients associated with each scenario were observed within their respective date ranges. Gaps where CTGs were not observed were not included in duration calculations.

• Observation dates denote the first date in which CTGs associated with breakaway infiltration were observed.

References

Fausto, R. S., Box, J. E., Vandecrux, B., van As, D., Steffen, K., Macferrin, M. J., Machguth, H., Colgan, W., Koenig, L. S., McGrath, D., Charalampidis, C., Braithwaite, R. J.: A snow density dataset for improving surface boundary conditions in Greenland ice sheet firn modelling, Front. Earth Sci., 6, https://doi.org/10.3389/feart.2018.00051, 2018.

Herron, M. M., & Langway, C. C.: Firn Densification: An Empirical Model, J. Glaciol., 25, 373–385, https://doi.org/10.3189/s0022143000015239, 1980.

Howat, I. M.: Temporal variability in snow accumulation and density at Summit Camp, Greenland ice sheet, J. Glaciol., 68, 1076–1084, https://doi.org/10.1017/jog.2022.21, 2022.

Lehning, M., Bartelt, P., Brown, B., Fierz, C., and Satyawali, P.: A physical SNOWPACK model for the Swiss avalanche warning Part II. Snow microstructure, Cold Reg. Sci. Technol., 35, 147–167, 2002b.

McDowell, I. E., Keegan, K. M., Wever, N., Osterberg, E. C., Hawley, R. L., & Marshall, H. P.: Firn Core Evidence of Two-Way Feedback Mechanisms Between Meltwater Infiltration and Firn Microstructure From the Western Percolation Zone of the Greenland Ice Sheet, J. Geophys. Res. Earth Surf., 128, https://doi.org/10.1029/2022JF006752, 2023.

Noël, B. P.: Rapid ablation zone expansion amplifies north Greenland mass loss: modelled (RACMO2) and observed (MODIS) data sets, PANGAEA, 2019.

Saito, J., Harper, J., and Humphrey, N.: Uptake and Transfer of Heat Within the Firn Layer of Greenland Ice Sheet's Percolation Zone, J Geophys. Res. Earth. Surf., 129, https://doi.org/10.1029/2024JF007667, 2024.

Steffen, K., Vandecrux, B., Houtz, D., Abdalati, W., Bayou, N., Box, J. E., Colgan, W. T., Espona Pernas, L., Griessinger, N., Haas-Artho, D., Heilig, A., Hubert, A., Iosifescu Enescu, I., Johnson-Amin, N., Karlsson, N. B., Kurup Buchholz, R., McGrath, D., Cullen, N. J., Naderpour, R., Molotch, N. P., Pedersen, A. Ø., Perren, B., Philipps, T., Plattner, G. K., Proksch, M., Revheim, M. K., Særrelse, M., Schneebli, M., Sampson, K., Starkweather, S., Steffen, S., Stroeve, J., Watler, B., Winton, Ø. A., Zwally, J., and Ahlstrøm, A.: GC-Net Level 1 historical automated weather station data, 2022.